A methodology for the shape optimization of flexible wings

M. Vázquez, *A. Dervieux, and †B. Koobus‡

May 12, 2006

Abstract

In this paper, we propose a methodology for the shape optimization of flexible wings. This methodology is based on a loosely coupling between a high-fidelity aeroelastic analyser and an aerodynamic optimizer. The shape update is formulated in a CAD-free representation, and a transpiration-based optimization is performed using an exact gradient method with a single adjoint state. The iterative process yields optimal shapes in the at-rest condition (i.e. with the aeroelastic deformations substracted). This shape optimization methodology is applied to the reduction of the sonic boom production while preserving the aerodynamic performances of wings, taking into account the aeroelastic deformations suffered by wings in flight conditions. With this end in view, the objective function model contains both aerodynamic parameters and an acoustic term based on the sonic boom downwards emission. Applications to the optimization of a supersonic civil jet wing and the AGARD Wing 445.6 are presented. The aeroelastic effects on the final optimized shapes are clearly apparent. We also observe that the convergence towards the optimal shapes is obtained after few optimization/aeroelastic coupling iterations.

1 Introduction

The design process of aircrafts still remains a challenging task due to the many interrelated requirements and constraints relative to loads, flutter, stress, dynamics, weight, etc. that enter in such complex problems [1, 2]. While the complete design of aircraft in aerospace industry is mainly achieved through analyses, tests, databases and skill of engineers, numerical optimization represents a promising approach for reducing cost and time of aerospace design process [3].

Numerous algorithms are proposed in the literature for optimizing the shape of aircrafts under aerodynamic analysis. However, such optimal shape design methods should consider structural weight and aeroelastic effects in order to be more relevant, specially for industrial aerospace design investigations. Structural weight affects lift and drag, and aeroelastic deformations change the aerodynamic shape [4]. In order to compensate the aeroelastic effect, a normal industrial practice is to design shapes using a jig-shape approach, that is considering a-priori the aeroelastic deformations so that the desired cruise shape is produced. This can be done by substracting the aeroelastic deformation from the original "at-rest" shape. The resulting shape can then be optimized in order

*INRIA, 2004 Route des Lucioles, BP. 93, 06902 Sophia-Antipolis, France

†INRIA, 2004 Route des Lucioles, BP. 93, 06902 Sophia-Antipolis, France

‡Université de Montpellier II, Dept Mathématiques, CC.051, 34095 MONTPELLIER Cedex 5, France, and INRIA

to satisfy the other design objectives. At first sight, this simplifies the multidisciplinary optimization process, for which any simplification is wellcome because of the dramatic complexity of aircraft design (see the authoritative [5]). However, jig-shape corrections are likely to fall short in the case of very long-range flight or high-speed one. A clear example concerns supersonic jets, where a trade-off between subsonic and supersonic regimes design has to be done since the aeroelastic response is different for both flow regimes.
In this paper, we propose a shape optimization methodology of flexible wings, which takes into account the aeroelastic deformations suffered by wings in flight conditions. This optimization methodology can be useful to analyze flexible wing performances, particularly when integrated to a multipoint shape optimization process involving aeroelastic analyses. In this work, we consider two situations: at-rest or landed (no forces act on the structure), and at cruise flight (steady aerodynamic forces act on the structure).
A common practical strategy to solve aeroelastic shape optimization problems is the Multidisciplinary Design Optimization (MDO) approach [4], "a methodology for the design of systems where the interaction between several disciplines must be considered, and where the designer is free to significantly affect the system performance in more than one discipline". In this kind of multidisciplinary approach, the optimization problem is coupled in a tightly manner, that is the coupled aerodynamic and structural problems are solved simultaneously [6, 7]. Mainly, three alternative formulations can be found in the literature according to the feasibility maintained at each optimization iteration of an MDO procedure [6] : the Multidisciplinary Feasible approach (MDF), the Individual Feasible approach (IDF), and the All at Once approach (AAO). In the MDF alternative, the complete multidisciplinary analysis is performed at each iteration of the optimizer. In the IDF approach, the aerodynamic and structural analyses are maintained at each optimization iteration, but the interdisciplinary coupling is not correct until optimization convergence. In the AAO approach, the individual analysis discipline equations are guaranteed only at optimization convergence. A drawback of the AOO and IDF alternatives is that no meaningful information may be availabe if the optimization procedure is stopped short of convergence.
An important and difficult point in MDO approach, is the efficient computation of the coupled model sensitivities. Its evaluation for aeroelastic coupling is a very complex matter (see for instance [8, 9, 10]). This point is common to all MDO problems: the need for evaluating the dependence between the different disciplines acting in the optimization process, which is expressed through an objective function. For instance, in the case of aeroelastic optimization problems, this function typically contains aerodynamic performance or flight condition related terms (lift/drag, sonic boom production, angle of incidence, etc.) and it may also contain structural ones (internal stresses, elastic model parameters, etc.). In [10], this sensitivity evaluation is simplified using a reduced model for the structural behaviour based on the Global Sensitivity Equations (GSE) proposed in [11] and which allows to evaluate the total sensitivity derivatives linking loads and deformations. Optimization methods based on GSE approach are also used in many other works [12, 13, 14]. One drawback of GSE based approaches is that all source codes must be open to analysis and modification in order to properly evaluate the off-diagonal sensitivities, which renders the schemes less flexible and limits their migration out of academic environments (see for instance [15]).

In this paper, we propose a different approach in which the aeroelastic response is detached from the optimization model in a loosely coupled way. The cost function to minimize does not include structure related terms, being the optimization performed only on the aerodynamic side and the aeroelastic response computed from the loads evaluated on the optimized shape. Therefore, following the aforementioned definition this kind of approach cannot be strictly considered as MDO since it performs multidisciplinary anaysis but only single disciplinary optimization. These approaches have the interesting feature to propose, at a rather low cost and implementation effort, solutions

for shape optimum design problems which take into account aeroelastic effects without computing the coupled aerodynamic-structural sensitivities. Moreover, in the proposed optimization algorithm, the aeroelastic analyser and the aerodynamic optimizer can be used as black-boxes, which renders this approach very modular and flexible. For these reasons, they are preferred for complex problems, as noted in reviews like [3, 16, 17]. Other loosely coupled schemes are also applied for instance in [3, 18, 6].

Particularly, the proposed optimization strategy is based on a global cycle which involves an aeroelastic analysis and optimization iterations over the aeroelastic deformed shape of the current cycle. The chosen strategy can be compared to the previously described MDF approach in the sense that the complete multidisiplinary analysis is performed before the optimization phase, so that stopping this coupled aerodynamic optimization/aeroelastic process short of convergence could yield useful design improvement. The aerodynamic optimizer, which was introduced in [19, 20], uses transpiration conditions and a "CAD-free" approach (according to the terminology given in [21]) to minimize the sonic boom downwards emission and to improve the aerodynamic properties of the aeroelastically deformed shapes. The aeroelastic response is in turn computed with a loosely coupled scheme in which high-fidelity aerodynamic and structural analysers are used on dynamic meshes, which follows [22].

The proposed shape optimization methodology is applied to the minimization of an objective function which is not only based on aerodynamic parameters but also on a sonic boom production term. Sonic boom optimization is of the utmost importance for future supersonic civil jets (and already for present ones: Concorde flights over land were worldwide banned due to sonic boom).

Sonic boom is the ground signature of the pressure shock produced by an aircraft flying at supersonic speed [23, 24]. Any solid body moving at supersonic speed develops a shock ahead that moves with it. For airplanes, this feature becomes a complex shock system (Fig. 1). This ground signature is responsible for structural damage in buildings, strong environmental impact, psychological effects on human beings in the area, and so on. It is not possible to escape to sonic boom production (except for no-lift bodies, which are not an issue of aircraft industry...) because lift force has to be transmited to the ground. Many solutions have been proposed to reduce it directly or to reduce its effects. In [19, 20] we have used an optimal shape design approach to reduce what we call **Sonic boom downwards emission (SBDE)** defined as the pressure gradient strength, measured as a volume integral inside a "box" right below the aircraft, namely it corresponds to the **near field** pressure shock system. We have shown in previous works [19, 20] how a reduction in the SBDE results can result in a reduction of the ground signature, based in our own results and from the analysis of other works.

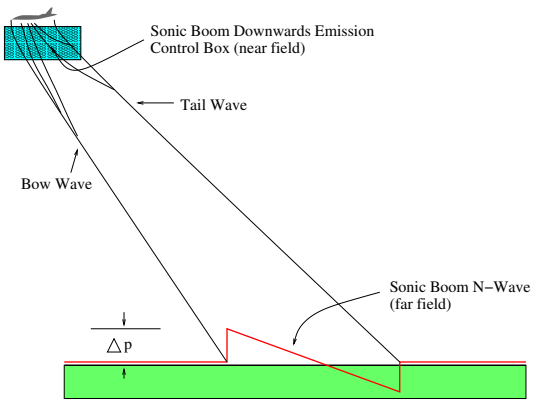

Figure 1: The sonic boom (simplified case of a N-wave). Sketch of near and far field shock wave patterns of a supersonic aircraft.

The remainder of this paper is organized as follows. Section 2 presents the three modules used in the coupled aerodynamic optimization/aeroelastic process: the aeroelastic analyser, the aerodynamic optimizer and the remeshing module. Section 3 describes the optimization/aeroelastic coupling strategy. Applications to the optimization of a flexible supersonic civil jet wing and the AGARD wing 445.6 are presented in Section 4. Finally, we draw some conclusions and perspectives in Section 5.

2 Shape optimization methodology: main options

The *problem to solve* is formulated as follows:

- the *central parameter* is the shape of the *at-rest* obstacle Γ, surrounding a structure, and surrounded by a flow. By "at-rest", we mean that the flow pressure will finally deform the elastic obstacle.

- as a function of Γ, the *state* of the system to optimize is the solution $(q(\Gamma), w(\Gamma))$ of a static coupled fluid-structure interaction. The variable $q(\Gamma)$ denotes the displacement of the structure, defining a deformed obstacle, and the variable $w(\Gamma)$ is made of the flow variables, defined on a domain surrounding the deformed obstacle.

- an objective functional is computed in terms of the parameter Γ through the state variables q and w:

$$j(\Gamma) \quad = \quad J(q(\Gamma), w(\Gamma)) \ .$$

- the target is to find the optimal at-rest shape $\Gamma_{opt} \ = \ Argmin \ \ j(\Gamma)$ subject to some contraints which can concern shape or state variables.

We observe that both shape update and structural deformation influence the domain occupied by the flow. It can be of interest to be able to handle in a common representation both shape updates and elastic obstacle deformations.
The first fundamental option of the proposed method is to formulate shape update in a CAD-free representation, as in [21, 20]. In short, this means that the shape is described by the position of *all* the vertices of a surfacic mesh. With this option, the elastic deformation will be also described by an update of the position of the same vertices (although they can be computed with a finite-element analysis relying on a different mesh).
As a result, we can make the *sum* of a shape update and an elastic deformation.

We now analyse further the state system. It writes in the continuous case as a two field problem, the first field is the structure, and the second one the fluid. However, if the structure can be set in a Lagrangian framework, this should not be done for the fluid. In the case of an Euler fluid model, a fixed-domain tranpiration-condition can be considered, but our experience is that this is not enough accurate. Taking the option of a variable mesh computed by an extra system, the state of the system becomes a *three-field coupled aeroelastic system* [25] involving:

- equations of structural equilibrium,

- fluid mesh equations,

- steady Euler fluid equations.

For a given shape parameter this system defines a state and we derive a value of the objective functional. In order to minimize (at least locally) this functional, we consider the application of an exact gradient method. The best strategy is to compute

an adjoint. Now this adjoint is necessarily a coupled three-field adjoint:

- structural adjoint equilibrium,

- fluid mesh adjoint equations,

- linearised-Euler adjoint equations.

We refer to [12] for such a tightly coupled optimization approach. Now, in many application the tightly coupled method can be costly and complex to develop. The main idea of the present paper is to exploit the following point:

In order to solve the aeroelastic optimization problem, it is enough to compute a couple of shapes (γ_1, γ_2) *such that :*

(i)- γ_1 *is a shape optimizing the functional in the limit case where elastic deformations are neglected (rigid fixed body),*

(ii)- optimal shape γ_1 *is the result of aeroelastic deformations represented by shape* γ_2*.*

Each of these steps can need a two-field adjoint system. Step (ii) is an inverse problem for the aeroelastic coupling. This can be solved simultaneously with optimization Step (i):

Find γ_1 *solution of (i) with a single-disciplinary optimization while computing at the same time its undeformed shape* γ_2 *with an aeroelastic analysis.*

If the variable domain is implemented with a variable mesh, then the single-disciplinary state system has to be formulated in terms of a coupled system of two fields, the flow field, and the mesh deformation field. For Euler flows, a way to reduce it to a single field state system, consists in representing the domain variation with a transpiration condition. This approximation carries several disadvantages. The main disadvantage is that the error is large when the domain variation is large. To overcome this, we can either restrict to small domain variations, or to apply a fixed point transpiration-deformation algorithm between:

- transpiration-based optimization,

- a remeshing by mesh deformation which produces a mesh fitted with the current domain.

The output of this algorithm is two-fold, first a shape that is optimal with respect to an infinitely-small transpiration perturbation, and, second, a flow that is computed on this shape without any transpiration error. We can also notice that the transpiration-based optimization step can be applied with an exact gradient method using a single adjoint state, the adjoint to the Euler system.

Then we can imagine a loop involving an alternation between the aeroelastic analysis and the fixed point transpiration-deformation method.

For the sake of accuracy, we think it is mandatory to use deformation also into the aeroelastic analysis (without any tranpiration step). Then, in the coupled algorithm, we shall not couple a deformation-based aeroelastic phase with the above fixed point transpiration-deformation optimization. Instead, **without changing the final optimal result**, we can account for the deformation/remeshing subphase inside the aeroelastic phase.

The global algorithm then writes in short:

1- Start with an initial shape,

2- Aeroelastic analysis including remeshing,

3- Transpiration-based optimization.

4- If residuals of 2 and 3 are not small, go to 2.

REMARK 1: In an inverse identification of the non-deformed shape (jig shape methods), the final shape may not satisfy some a priori specifications. In the proposed approach, we can take into account some constraint on shape or a particular parametrization with CAD variables. It is enough to introduce this in the optimization phase. But the whole algorithm turns on the CAD-free variables.

The next section is devoted to the practical implementation of this global algorithm.

3 A three modules scheme

The coupled optimization/aeroelastic problem involves two main phases, that repeat iteratively until a convergence criteria is achieved. Each phase corresponds to a different module, a third module is used to link them together. To an **aeroelastic analysis** phase follows an **aerodynamic optimization** one. The connecting module is a **remeshing tool**, that translates the discretized surface corrections resulting from the optimization phase into a modified fluid volumic mesh that feeds the aeroelastic analysis module. In brief, the three modules that constitute the integrated aeroelastic optimization scheme are:

- **The aeroelastic analysis module:** a loosely coupled fluid-structure solver $\Phi(\Omega, \Sigma)$.
- **The aerodynamic optimization module:** an aerodynamic optimizer $\Upsilon(n, \Omega)$.
- **The remeshing module:** a remeshing tool $\Xi(\gamma, \Omega)$.

The inputs of all the previous modules contain $\Omega \in \mathbb{R}^{3\times N^{\text{vol}}}$. This notation is used for the discretization of the complete fluid domain, where N^{vol} is the total number of nodes in the volumic mesh. We will also distinguish the **at-rest** meshes from the **cruise** ones, noted $\widehat{\Omega}$ and $\overline{\Omega}$ respectively. The former ones are equivalent to the shapes at-rest, optimized or not. The cruise meshes are those following the shape aeroelastic deformations, also optimized or not. This is very important, because by saving separately optimization and aeroelastic modifications, the original shapes can be recovered after the coupled optimization. In brief, we are interested in how the final shapes will look like at-rest. An additional input item is $\Sigma \in \mathbb{R}^{3\times N^{\text{stru}}}$ which corresponds to the structure grid The structural model is a linear one, like that of [12, 22]. Typically, $N^{\text{stru}} << N^{\text{vol}}$, which renders the structural problem much smaller and cheaper than the fluid dynamics one. The grid notation is summarized as follows: the **at-rest volumic meshes** are noted $\widehat{\Omega}$, the **at-rest structure meshes** are noted $\widehat{\Sigma}$ and the **cruise volumic meshes** are noted $\overline{\Omega}$. Let us depict each of the modules.

3.1 The aeroelastic analysis module $\Phi(\Omega, \Sigma)$

Fluid-Structure Solver $\Phi(\hat{\Omega}, \hat{\Sigma})$

Inputs:

$\widehat{\Omega} \in \mathbb{R}^{3 \times N^{\text{vol}}}$, *at-rest* fluid mesh

$\widehat{\Sigma} \in \mathbb{R}^{3 \times N^{\text{stru}}}$, *at-rest* structure mesh

Output:

$\overline{\Omega} \in \mathbb{R}^{3 \times N^{\text{vol}}}$, *cruise* fluid mesh

`Compute the deformed fluid mesh` $\overline{\Omega}$`, coming from the fluid-structure coupling:`

$$\overline{\Omega} = \Phi(\widehat{\Omega}, \widehat{\Sigma})$$

The aeroelastic module, developed by Ch. Farhat's group at the university of Colorado at Boulder in cooperation with INRIA, is based on the methodology introduced in [22, 25]. The solution of the coupled fluid-structure problem is computed by a staggered solution procedure in time [26]. This scheme is also used in [12] for computing the aeroelastic response of various wings in aeroelastic optimization problems. This kernel yields a coupled fluid-structure static analysis based on a pseudo time advancing scheme with two stages: a fluid evaluation stage followed by a structural computation, based on the pressure distribution given by the preceding fluid simulation.

The problem of the motion of the fluid/structure interface that occurs in coupled aeroelastic problems is addressed by solving the fluid equations on deformable dynamic meshes. An Arbitrary Lagrangian Eulerian (ALE) [27],[22] formulation is used in order to perform the integration of the fluid equations on a moving mesh. The coupled aeroelastic problem to be solved can then be viewed as a three-field problem [25],[22]: the fluid, the structure and the dynamic mesh which is represented by a pseudo-structural system. The semi-discrete equations governing the three-way coupled problem can be written as follows:

$$\begin{aligned} \frac{\partial}{\partial t}(V(x,t)w(t)) + F^c(w(t), x, \dot{x}) &= R(w(t), x) \\ M\frac{\partial^2 q}{\partial t^2} + f^{int}(q) &= f^{ext}(w(t), x) \\ \tilde{M}\frac{\partial^2 x}{\partial t^2} + \tilde{D}\frac{\partial x}{\partial t} + \tilde{K}x &= K_c q \end{aligned} \tag{1}$$

where t designates time, x the position of a moving fluid grid point, w is the fluid state vector, V results from the finite element/volume discretization of the fluid equations, F^c is the vector of convective ALE fluxes, R is the vector of diffusive fluxes, q is the structural displacement vector, f^{int} denotes the vector of internal forces in the structure, f^{ext} the vector of external forces, M is the finite element mass matrix of the structure, $\tilde{M}$, $\tilde{D}$ and $\tilde{K}$ are fictitious mass, damping and stiffness matrices associated with the moving fluid grid and K_c is a transfer matrix that describes the action of the motion of the structural side of the fluid/structure interface on the fluid dynamic mesh.

At the discrete level, a mesh conforming to the structure deformation is built by moving the vertices with a pseudo-structural model [28]. Then the flow is advanced on this mesh. More specifically, the compressible flow Euler equations are discretized

by a Mixed Element-Volume method (see for instance [29]) which involves a second-order space-accurate scheme based on Roe's solver. Next, at the structural stage, the pressure loads are applied to the structure and the resulting structural displacements are computed. In this work, the structure is represented by a finite element model of a flat plate embedded in the wing, which is a simplified model of the internal structure. The displacements are finally transferred to the wet surface of the wing, producing a deformed volumic mesh. After convergence towards the static aeroelastic response, this volumic mesh is the output of the aeroelastic analysis module.

3.2 The aerodynamic optimization module $\Upsilon(n, \bar{\Omega})$

Aerodynamic Optimizer $\Upsilon(n, \bar{\Omega})$

Inputs:

n, number of optimization iterations

$\overline{\Omega} \in \mathbb{R}^{3 \times N^{\text{vol}}}$, cruise fluid mesh

Output:

$\gamma_n \in \mathbb{R}^{N^{\text{skin}}}$, shape correction

`Do` $nc = 1, n$

- `Compute state` $w(\overline{\Omega})$ `and adjoint` $\Pi(\overline{\Omega})$`, compute the gradient` $g(\gamma_{nc}, w(\overline{\Omega}), \Pi(\overline{\Omega}))$
- `Compute the preconditioner` P^*
- `Compute` ρ `(internal cycle)`
- `Update the shape correction:`

$$\gamma_{nc} \;=\; \gamma_{nc-1} - \rho \quad P^* \;\; g(\gamma_{nc}, w(\overline{\Omega}), \Pi(\overline{\Omega}))$$

`Next` nc

The optimization algorithm is designed to reduce the **sonic boom downwards emission** while preserving some aerodynamic performances (basically lift and/or drag), see [19, 20]. It is a **CAD-Free** based algorithm (these algorithms are also known as "discrete approaches" [30]) : the design parameters space is set by the physical positions of each of the skin discretization nodes placed on the shape to be optimized. Here, the shapes derived from the iterative optimization process are characterized using a **transpired perturbation**, noted as γ. A scalar which corresponds to a (small) displacement in the normal direction is assigned to each skin node. Therefore $\gamma \in \mathbb{R}^{N^{\text{skin}}}$, where N^{skin} is the number of skin nodes on the optimization's target shape. In order to handle a larger number of design parameters, an adjoint problem is built (see [31]) based on the computation of a **discrete adjoint** ([32], [33]). It is of paramount importance that the optimization process has a mesh-size independant convergence for dealing efficiently with large design problems. To this end, we apply the multilevel preconditioner analysed and developed in [34] and successfully used in [19, 20], which filters high-frequency oscillations typically seen in other CAD-free approaches.

The optimizer inputs are the number n of iterations and a given initial volumic mesh Ω. As for the aeroelastic analysis module, the optimizer can be fed either with a at-rest mesh $\widehat{\Omega}$ or a cruise one $\overline{\Omega}$. We have designed the full scheme considering that the input mesh of the optimizer is a cruise one $\overline{\Omega}$. Indeed, it is expected that the surface

deformations related to the optimization will be smaller than those coming from the aeroelastic coupling. The cruise mesh $\overline{\Omega}$ is then optimized as if was a rigid body.

After n iterations, a shape correction γ_n is produced, which represents a displacement of the boundary defining an optimum shape by means of the transpiration conditions (see [35] for instance). For each iteration nc, the state $w(\overline{\Omega})$, its adjoint $\Pi(\overline{\Omega})$ state and the cost functional gradient $g(\gamma_{nc}, w(\overline{\Omega}), \Pi(\overline{\Omega}))$ are sequentially computed. In order to get $w(\overline{\Omega})$, the discretized **compressible flow Euler equations** are solved by means of a Finite-Volume method and integrated using a second order space accurate Roe upwind scheme. The cost functional gradient is then calculated. The original cost functional was proposed in [19]. Here we have introduced some modifications to render it more efficient. It evaluates both the aerodynamic properties and what we call sonic boom downwards emission (SBDE):

$$j(\gamma) = \alpha_1 \ f_D{}^2 + \alpha_2 \ f_L{}^2 + \alpha_3 \int_{\overline{\Omega}^B} \frac{\partial p}{\partial x_i} \ \frac{\partial p}{\partial x_i} \ dV \tag{2}$$

where

$$f_D = \begin{cases} C_D - C_D^{target} & \text{if } \ C_D \geq C_D^{target} \\ \\ 0 & \text{otherwise} \end{cases}$$

$$f_L = \begin{cases} C_L - C_L^{target} & \text{if } \ C_L \leq C_L^{target} \\ \\ 0 & \text{otherwise} \end{cases}$$

in which α_1, α_2 and α_3 are constants that allow to vary the relative weight between the cost functional terms. These terms are related respectively to the aerodynamic performance (drag, lift) and SBDE. At least α_1 and α_2 should be both non-zero in order to avoid a trivial optimization problem. In practice, several refinements are necessary. In particular, moment should be maintained and drag should be minimized. The integration volume $\overline{\Omega}^B$ is a control box defined as a part of the computational domain located below the airplane. The functions f_D and f_L are zero when the drag is smaller than the target drag and when the lift is larger than the lift target, respectively.

The shape volume is conserved by sections, projecting the gradient on a volume preserving space [19]. In order to avoid volume "migration" from one end to the other for the optimized shapes, the whole volume can be divided in a certain number of sections, in general transversal to the spanwise direction. Therefore, each node i can be assigned to a section which contains $N(i)$ of them. The volume is then preserved individually for each section.

Although we prefer not to vary the incidence angle and therefore gaining lift only by cambering, we have also implemented a variable incidence equation , based on that of [36]. At each iteration n, the incidence angle θ is updated according to

$$\theta^{nc+1} = \theta^{nc} - \frac{1}{2} \ f_L^{nc}. \tag{3}$$

It takes profit of the linear dependence between the incidence angle and the lift coefficient for small incidences. It increases the incidence angle *only* when lift is lost between two iteration steps, namely when cambering fails to recover it.

3.3 The remeshing module $\Xi(\gamma, \Omega)$

Remeshing Algorithm $\Xi(\gamma_n^p, \overline{\Omega}^p)$

Inputs:

$\gamma_n^p \in \mathbb{R}^{N^{\text{skin}}}$, optimized shape correction at coupling iteration p

$\overline{\Omega}^p \in \mathbb{R}^{3 \times N^{\text{vol}}}$, cruise fluid mesh at coupling iteration p

Output:

$\overline{\Omega}^p_{\text{OPT}} \in \mathbb{R}^{3 \times N^{\text{vol}}}$, optimized cruise fluid mesh at coupling iteration p

`Move the input mesh` $\overline{\Omega}^p$ `according to` γ_n^p`:`

$$\overline{\Omega}^p_{\text{OPT}} = \Xi(\gamma_n^p, \overline{\Omega}^p)$$

The remeshing module works as an interface between the aeroelastic module and the optimization one. The aeroelastic module already includes the same remeshing algorithm to take into account the shape deformations. They are transferred to the optimization module as a modified volumic grid, called the cruise mesh $\overline{\Omega}^p$ for a coupling iteration p, suitable to be the optimizer input. On the other hand, the optimizer's output is a shape correction γ_n^p defined on the surface nodes according to the transpiration condition. Through a remeshing algorithm (e.g. [26] and [28]), a corrected volumic grid is produced, which will be used in turn as input by the aeroelastic module. The algorithm generates a new mesh by moving the nodes of the input mesh $\overline{\Omega}^p$ with a pseudo-structural model, under the constraint that the new boundary nodes are moved from the input ones according to the input shape correction γ_n^p.

4 The integrated aeroelastic optimization scheme

Optimization/Aeroelastic Coupling Algorithm

$\widehat{\Omega}^0$ = initial (pre-optimized) *at-rest* mesh

Do p (coupling iterations)

- Compute the aeroelastic coupling from the *at-rest* fluid mesh $\widehat{\Omega}^{p-1}$ and the *at-rest* structure mesh $\widehat{\Sigma}$, and obtain the intermediate *cruise* mesh $\overline{\Omega}^p$:

$$\overline{\Omega}^p = \Phi(\widehat{\Omega}^{p-1}, \widehat{\Sigma})$$

- Compute the optimum boundary correction γ_n^p by optimizing $\overline{\Omega}^p$, through n optimization iterations:

$$\gamma_n^p = \Upsilon(n, \overline{\Omega}^p)$$

- Compute the optimized *cruise* fluid mesh $\overline{\Omega}^p_{\rm OPT}$:

$$\overline{\Omega}^p_{\rm OPT} = \Xi(\gamma_n^p, \overline{\Omega}^p)$$

- Evaluate the *at-rest* optimized fluid mesh, namely $\widehat{\Omega}^p_{\rm OPT}$:

$$\begin{aligned} \Delta\widehat{\Omega}^p_{\rm OPT} &= \overline{\Omega}^p_{\rm OPT} - \overline{\Omega}^p \\ \widehat{\Omega}^p_{\rm OPT} &= \widehat{\Omega}^{p-1} + \Delta\widehat{\Omega}^p_{\rm OPT} \end{aligned}$$

- Set $\widehat{\Omega}^p = \widehat{\Omega}^p_{\rm OPT}$

Next p

As shown in the box above, the integrated scheme works through an iterative process that links at each iteration p the three modules (Φ, Υ, Ξ). There are two nested iterative cycles: a global **coupling cycle** and a nested **optimization cycle**. In the coupling cycle, the *Aeroelastic Module* Φ evaluates the shape's structural response to the surface pressure distribution, i.e. it computes the **cruise** configuration from the *at-rest* one. Then, the *Optimization Module* Υ modifies the cruise shape coming from Φ by performing n optimization iterations. That is to say, it optimizes the cruise configuration considering the wing as rigid and only under SBDE and aerodynamic constraints. The *Remeshing Module* Ξ is then applied to transform the transpired shape modifications γ in a fluid volumic grid. The final update is done by substracting the current structural deformation in order to obtain the new optimized at-rest grid, which is in turn given to the *Aeroelastic Module* to start a new coupling iteration $p+1$. For a faster convergence, the new iteration takes as initial geometry for the aeroelastic analysis the newly optimized at-rest configuration *plus* the aeroelastic deformation of the precedent step.

The fact that, on one side the aeroelastic analyser is based on an ALE formulation and dynamic meshes and on the other side the aerodynamic optimizer uses transpiration conditions and so fixed meshes, is not a weakness of the proposed approach. On the contrary, we show in this way that a viable optimization/aeroelastic coupling procedure can be built even when an aeroelastic analyser and an aerodynamic optimizer do not share the same description of the fluid equations, leading to handle dynamic and fixed computational grids in the coupling process.

In [12], an aeroelastic optimization scheme is divided in three stages: optimization, design and analysis. In our scheme, optimization and design stages are fused in one because the CAD-free optimization output is already an aerodynamic shape with the

required characteristics.

¿From the implementation side, we have observed that, at each coupling iteration p, it is very advantageous to keep the optimization modifications corresponding to iteration $p-1$ to evaluate the optimized $\gamma_n^p = \Upsilon(n, \overline{\Omega}^p)$. In this way Υ's input $\overline{\Omega}^p$ corresponds to the $p-1$ optimized shape with the corresponding p aeroelastic deformation. The starting point for the current Υ cycle is therefore closer to the following optimized state.

After n optimization iterations that introduce surface modifications γ_n through transpiration conditions, the *Remeshing Module* Ξ is called to deform the whole mesh while keeping the original topology. Then, Φ and Υ can be linked. As a bonus, their output mesh deformations can be saved independently at each iteration to keep track of the separate effects of aeroelasticity and optimization. This is particularly important in order to see what is the final shape of the at-rest optimized wing. The number of optimization iterations n can vary in order to improve the scheme's turnaround time. Indeed, a complete optimization convergence is not necessary in the first full scheme cycles.

By construction, the method that we propose seeks an optimal shape for the coupled fluid-structure system. Any fixed point of the algorithm will satisfy the optimality condition for the deformed shape. Furthermore, this optimality condition is checked with a mesh following the deformed geometry, and with, at convergence, a vanishing transpiration displacement. This implies that the transpiration approximation has only an influence on the optimality fulfilled condition, and not on the flow evaluation. Indeed, the flow evaluation does not suffer from transpiration inaccuracies since, with a zero displacement at convergence, the transpiration condition reduces to the usual slip boundary condition.

5 Numerical Examples

The scheme behavior is evaluated through two optimization problems: the delta wing of a Supersonic Business Jet (SBJ) projected by Dassault Aviation, and the AGARD wing 445.6.

The two main scheme features on which we focus are the following ones. On one hand, the scheme must be **convergent** in the sense that, as the coupling iterations go on, the geometries produced should converge to a limit shape. Both Φ and Υ deform shapes: Φ evaluates the structural response to a stationary flow solution and Υ corrects the surfaces after a given minimization objective. The goal is that, at the end, each of Φ and Υ must not undo what the other module has done before. A priori, this is not an obvious point. The wing downwards twist (the *washout*) in flight produces (i) a lift loss and (ii) a SBDE reduction. Then, the optimization process will try to recover from (i) while keeping an eye on (ii). Point (i) could be compensated by two means: cambering and incidence angle variation. But of course, this shape modification will have effects on the following structural response. We will show to which extent this combined effects are entangled. On the other hand, it is obvious that the scheme must be **useful**. What is the point in including the aeroelastic effects in an aerodynamic and sonic boom production optimization process? Clearly, both torsion and flexion do have an effect on the aerodynamic performance. The point is to assess its effect on the reduction of the sonic boom production.

For both applications,we first carry out some optimization iterations on the rigid wings, namely without aeroelastic deformations. The optimized (rigid) wings illustrate the performance of our aerodynamic and sonic boom production optimizer and its ability to reduce the SBDE while keeping the aerodynamic properties. As a second stage, we start a coupled aerodynamic optimization / aeroelastic analysis computation taking these initial geometries as initial condition.

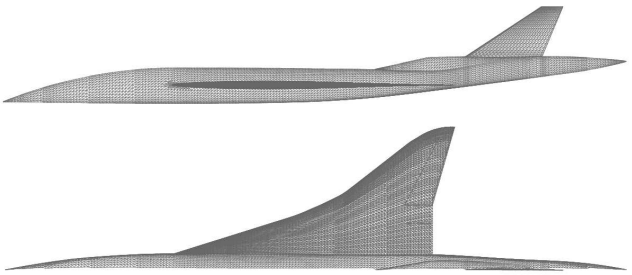

Figure 2: Dassault Aviation's Supersonic Business Jet. Side and upper views.

5.1 Dassault's Aviation Supersonic Business Jet wing

This first application concerns the SBDE reduction of the wing of a Supersonic Business Jet (SBJ) projected by Dassault Aviation, whom we are indebted for providing the geometry (Fig. 2). The aircraft isolated wings are depicted in Fig. 3.

As pointed out in our previous works, we proceed by optimizing the wings *separately* from the plane, as a first step. Then, we integrate the results to the full plane. In this paper, we will show the result of the optimization of the aircraft isolated wings depicted in Fig. 3.

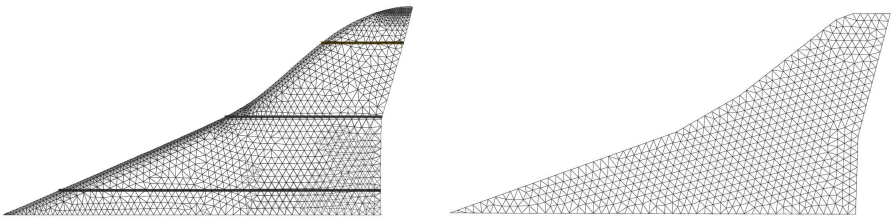

Figure 3: Dassault Aviation's Supersonic Business Jet. Left: Isolated wing discretization, showing the cross-sectional shapes (airfoils) considered (the thick horizontal lines): outboard, mid and inboard. Right: structural mesh (flat plate finite element model).

The baseline wings provided by the constructor for this generic geometry are horizontally symmetrical, with two different sweep angles of 17° and 38° respectively, and a rather smooth transition between them. The Mach angle for $M = 1.8$ is around 34°. Then, while the inboard part of the wings falls within the Mach cone (viz. [37]), producing a lower wave drag, the outboard wing cuts through the Mach cone. As a consequence, the sharpest pressure gradients are produced ahead of the outboard portion of the wing, being the main source of SBDE. The wing volumic mesh corresponding to Fig. 3 is made of 65418 tetrahedra (12963 nodes) and its surface mesh contains 4692 triangles (2408 nodes, which is the number of design parameters). The Mach number is set to 1.8 and the initial incidence angle is 3°.

For the aeroelastic simulations, we use a thin plate finite element model of the wing which contains 1286 triangular shell elements (Fig. 3, right). The properties of the material (Young modulus, Poisson coefficient, thickness and density) have been calibrated so that realistic displacements, eigenmodes and eigenvalues are recovered. This simple structural model is sufficient for our purpose since, in our design process, we are interested by taking into account the aeroelastic effect but not the structural optimization of the wing.

5.1.1 Initial rigid optimization

The double delta wing renders optimized shapes that are very different than those of more simple forms. The fact is that the wing inboard produces a much lower pressure gradient due to its sweep angle, which is smaller than that of the Mach cone. Therefore, while the shape modifications that reduce the SBDE tend to focus on the outboard half, the lift can be recovered by cambering the inboard region. This effect is naturally developed by our algorithm. After optimization, the wing profiles at different locations in the wing-span direction show different forms, depending on its position relatively to the fuselage. Fig. 4 shows the three wing cros-sectional cuts of Fig. 3, left. After 30 optimization cycles and using a **volume preserving projected gradient (VPGP)** strategy [19] that preserves the volume per-wingspan-section (40 sections in this case), the outboard profile develops a flattened downwards half and a sharp leading edge. On the other hand, in the inboard one this effect is much less evident. The mid-section profile shows a combination of those effects, stronger perhaps for the SBDE reduction than for the lift recovery. Some very slight wiggles appear on the optimal shapes. that would be easily mastered with a smoother parametrization as in [38].

Fig. 5 illustrates the SBDE reduction, as the pressure distribution in a plane below the wing. Note the pressure peak location for the original wings. As addressed in [19], this is a strong reason for not using a propagation code, in order to evaluate the ground pressure signature, that only considers as input what happens in a line contained in the aircraft symmetry plane in order to evaluate the ground pressure signature . Unless a refined volumic grid is used, adapted to follow the strong shock produced *below* the wing and *out of* the symmetry plane, the pressure signature so computed will be only that of the fuselage. This point leads us to believe that this kind of propagation methods present an important drawback: they are strongly sensitive to the position of the line used to take the input pressure distribution.

5.1.2 Optimization/Aeroelastic coupling

We proceed to compute the coupled optimization from the optimized rigid wing as initial geometry. As said above, the flexion and torsion of the delta wing is stronger in the outboard part, which is in turn responsible for the largest amount of SBDE production. In fact, this deformation reduces it. Fig. 7 shows the evolution of different parameters with the coupling iterations. Each of the curves is plot from the values taken at the optimization iterations performed by the aerodynamic optimizer. These plots clearly illustrate the effect of aeroelasticity. The rigid wing optimization is labelled as the "Coupling iteration 1". This first iteration carries the heaviest part of the optimization, because it runs the full way from the original wing to the optimized one. Approximately after 20 optimization iterations, the lift is stabilized at the target value and the SBDE cost (defined as the third term of cost functional definition (2)) is reduced by almost 40%. As said above, the incidence angle does not change because cambering is enough to recover the lift.

The next coupling iteration takes into account the aeroelastic deformation suffered by the optimized rigid wing. The convergence is in this case much faster. In five optimization iterations, the lift and SBDE terms of the cost functional stabilize. The lift is in this case regained by changing the incidence. In any case, this parameter is also stable after five iterations. This optimization stage has to recover about 20% of the lift, lost because of the aeroelastic deformations. On the other hand, the SBDE has accordingly been reduced. Then, the objective is double: to recover the lift up to the value of the *rigid* optimized one and to further reduce the SBDE of the *deformed* wing. The SBDE reduction will not be so intense because most of the work has been done in the initial optimization, namely the rigid one. Basically, it can be said that the rest of the work consists in recovering the lift under the SBDE constraints. The next 4 coupling iterations have progressively smaller effect, converging to the lift target, effectively reducing the SBDE and stabilizing the incidence angle around 3.1°.

On the aeroelastic analysis side, we have observed that the loosely coupled scheme

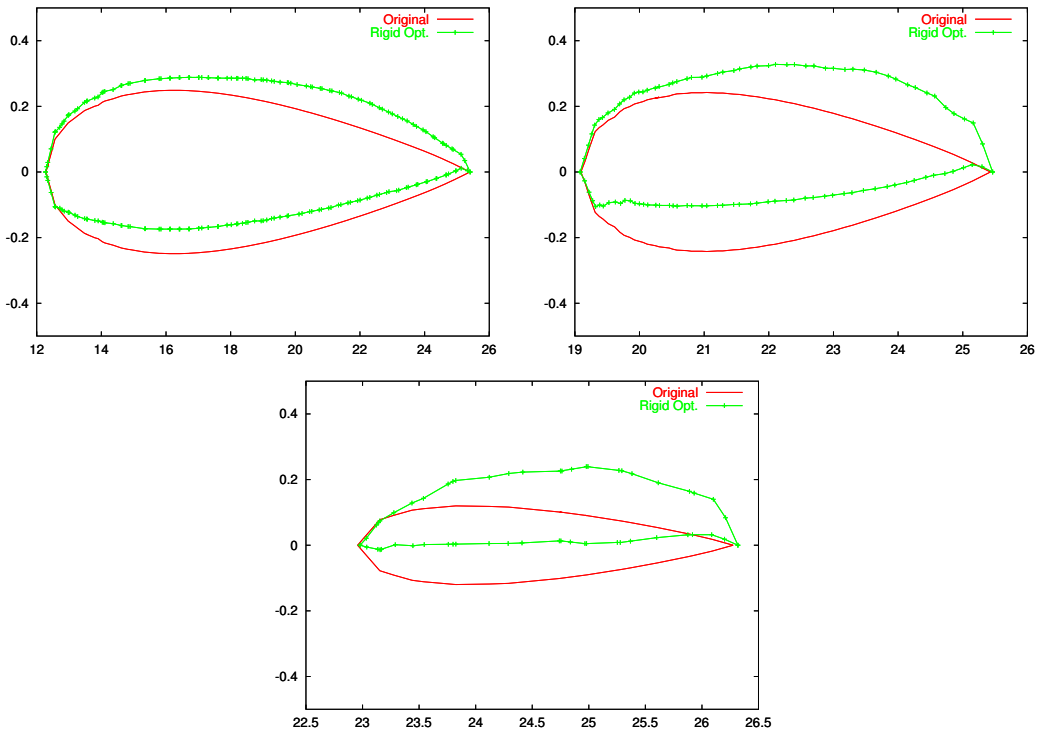

Figure 4: Dassault Aviation's Supersonic Business Jet. Non-coupled optimization of a rigid wing. From left to right and from top to bottom: inboard, midboard and outboard aircraft wing airfoils.

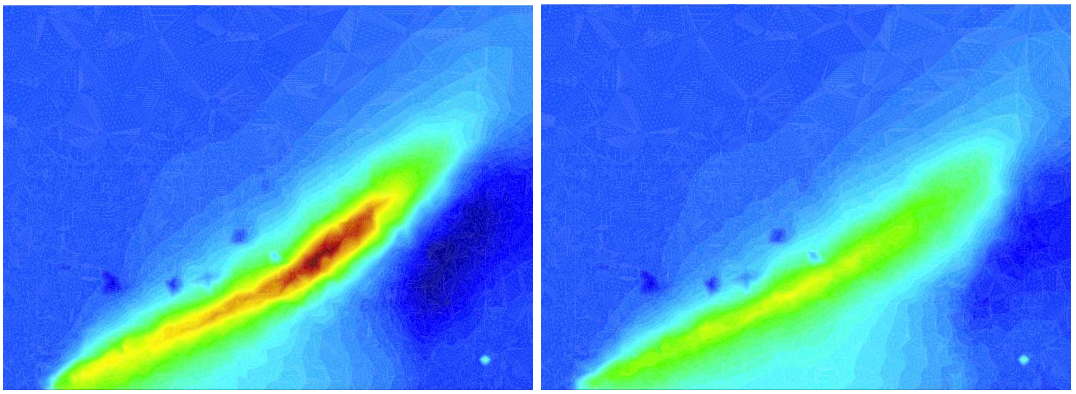

Figure 5: Dassault Aviation's Supersonic Business Jet. Non-coupled optimization of a rigid wing. Pressure distribution for a plane below the original and optimized wings, left and right respectively.

we used allows to obtain a convergent displacements norm, as seen in Fig. 6. We name ||MAD|| the **Mean Aeroelastic Displacement Norm**, that is to say the L^2 norm of the aeroelastic displacements divided by the number of the moving surface nodes, which is equal to the dimension of the optimization parameters space. In the same figure, we have also plotted the ||MOD||, the **Mean Optimization Displacements Norm** to see the scheme convergence and also to compare it with the ||MAD||.

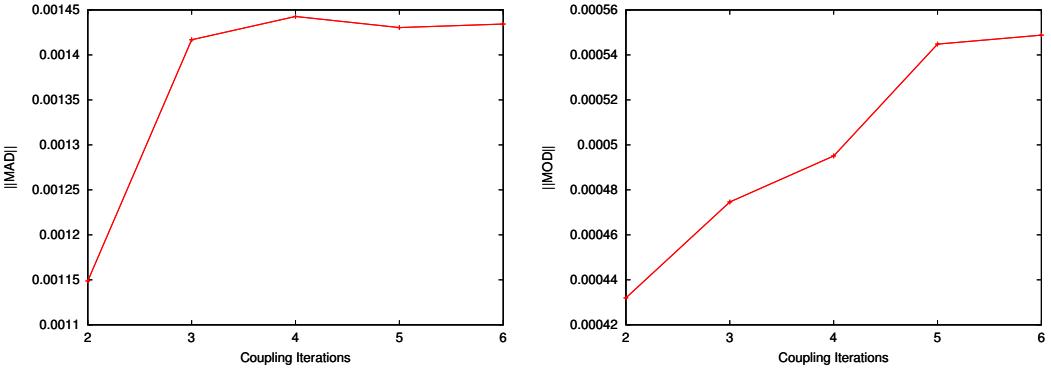

Figure 6: Dassault Aviation's Supersonic Business Jet. Convergence of the coupled algorithm. Evolution of the mean aeroelastic displacements (||MAD||) and the mean optimization displacements (||MOD||) with the coupling iterations.

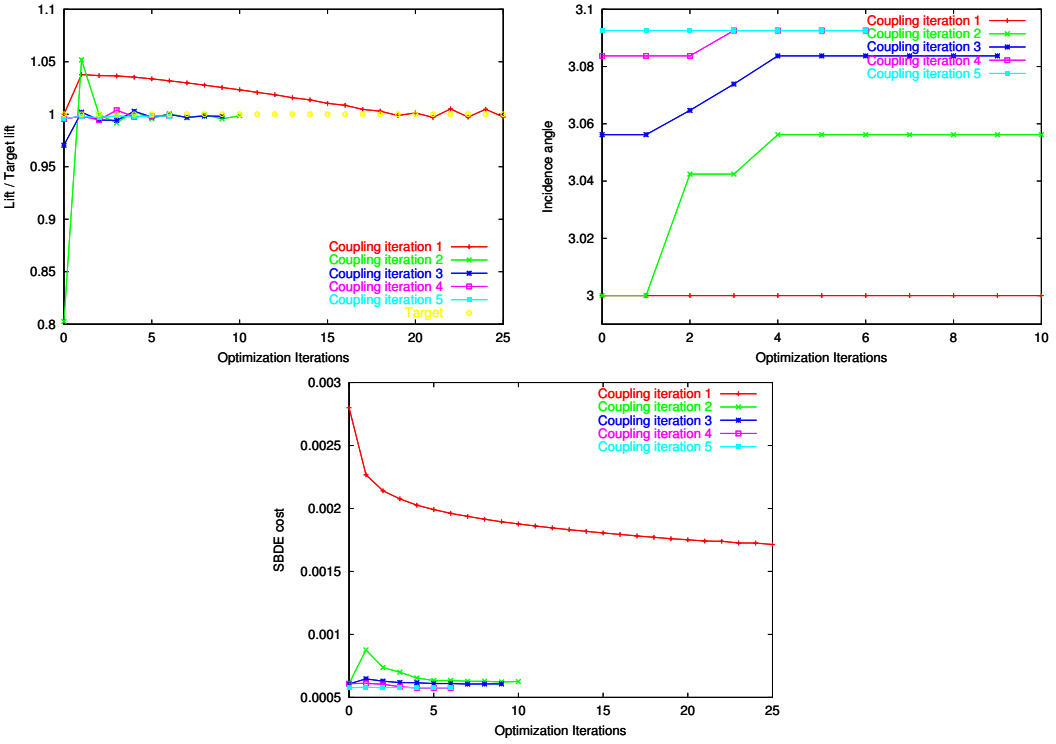

Figure 7: Dassault Aviation's Supersonic Business Jet. Convergence of the coupling algorithm. Evolution of different parameters with the coupling iterations.

The three optimized wing cross-sectional shapes of Fig. 4 are again shown in Fig. 8, but now including the plots corresponding to the coupling problem, in the "at-rest" and "cruise" configuration. Recall that the configuration "at-rest" is constructed from the "cruise" one (optimized or not) by substracting the aeroelastic displacements. In this way, the airfoil at-rest compares to the rigid one. The optimized inboard airfoil now presents a larger cambering to gain part of the lift lost by the wing torsion and flexion. The flattened down side is due to the combination of the upper side spread-out (because the volume must be conserved locally for the corresponding section) and the SBDE

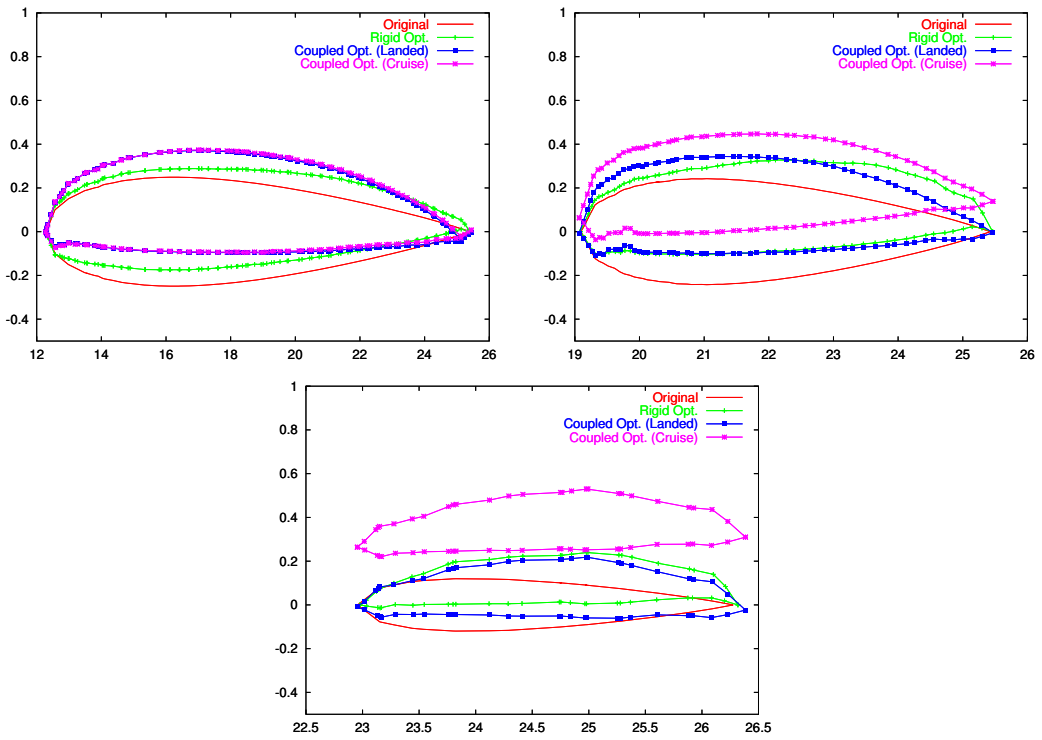

Figure 8: Dassault Aviation's Supersonic Business Jet. Optimized flexible wing. Clockwise: inboard, mid-wing and outboard cross-sectional cuts.

reduction. At this wing location, the aeroelastic deformation is very small. The middle section is much more influenced by the deformations, and the negative twist (smaller angle of attack at the tip than at the root of the wing) becomes apparent. ¿From the comparison of both at-rest airfoils, we observe how the method has compensated the twist effect (the wrinkled look is due to both the cutting process and the mesh coarseness). This fact is even clearer in the outboard airfoil. The optimized down sides for both the cruise-coupled and the rigid problems present almost parallel shapes. Consequently, the at-rest coupled-optimized airfoil is very different from that of the rigid problem.

5.2 AGARD wing 445.6

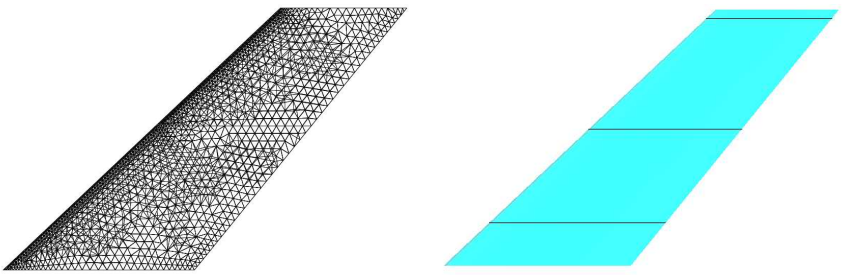

Figure 9: AGARD wing 445.6. Surface grid (left) and the three cross-sectional cuts.

We consider now the AGARD wing 445.6 whose geometry is described in details in [39]. Flows around this structure have been measured for Mach as high as 1.14.

Due to the high flexibility of the weakened structural model 3 of [39], this second calculation represents a relevant test case for evaluating the method behavior in the case of larger displacements, from the fluid standpoint.

¿From the structural standpoint, the linear structural analysis is chosen identical to the one applied in the previous case. However, for a real world application, the non-linear approximation would be more appropriate.

The three dimensional unstructured CFD mesh contains 9505 nodes and 43973 tetrahedra. The wing surface (Fig. 9) to optimize contains 5488 triangles and 2782 grid points, which is in turn the dimension of the parametrization space according to our CAD-free approach. The Mach number is set to 1.8 and the initial incidence angle is 3°.

For the aeroelastic analysis, the structure of the wing is discretized by a thin plate finite element model which contains 800 triangular composite shell elements and is based on the information given in [39].

5.2.1 Initial rigid optimization

In this first step, we have performed 20 optimization iterations. As in the previous application, this does not exhaust the optimization process for the rigid wing, but provides a good initial geometry for the coupled case. We have applied the VPGP strategy defined in Sec. 4.1.1, in order to keep constant the volume of 60 wingspan sections. Unlike the delta wing, the *rigid* AGARD wing produces basically the same shock strength all along its length. Therefore there is no outboard-inboard volume migration. However, this is very important for the *aeroelastic* case, and therefore the VPGP-by-sections solution is always adopted. We let the incidence angle vary according to (3), although for the rigid optimization the optimizer manages to preserve the lift only by cambering the wing. The α weight parameters in the cost functional (2) are set to $\alpha_1 = 10.0$, $\alpha_2 = 100.0$ and $\alpha_3 = 1.0$. The target lift and drag coefficients are respectively that of the original wing and half of it, evaluated at the initial incidence angle.

Fig. 10 (left) shows the optimized wing mid-section compared to the original one. Fig. 11 illustrates the effect of optimization on the SBDE by depicting the pressure distribution in a plane below the wing. Fig. 10 (right) shows the pressure along a line below the wing mid-section (Fig. 9, right). Although the final converged state is not yet completely reached, because this first rigid optimization is no more than a first iterate for the coupled process, the tendency can be clearly seen. By minimizing the SBDE, the resulting shapes have flattened downwards faces and sharper leading edges. The SBDE, measured as the integral of the pressure gradient below the wing, has diminished by rounding the main pressure peak and the following undershot. As reported in our previous works, this has the combined effect of (i) reducing the **pressure impulse**, (ii) reducing the initial pressure peak and (iii) introducing a **time delay** in the pressure rise. As shown in [19], this fact can be highlighted by computing the Euler flow around two 2-D profiles corresponding to the original and the optimized (rigid) wings.

5.2.2 Optimization/Aeroelastic coupling

The optimized rigid wing of the previous section is taken as an initial geometry for the coupled process.

Due to the imposed structural properties, this wing undergoes large and rather unrealistic displacements under the action of such a supersonic flow. Though a non linear analysis would have been more appropriate, the structural discretization is achieved by a linear finite element approach. Indeed, the main purpose of this application is to assess the method behavior, in particular its robustness and convergence, in the case of large displacements.

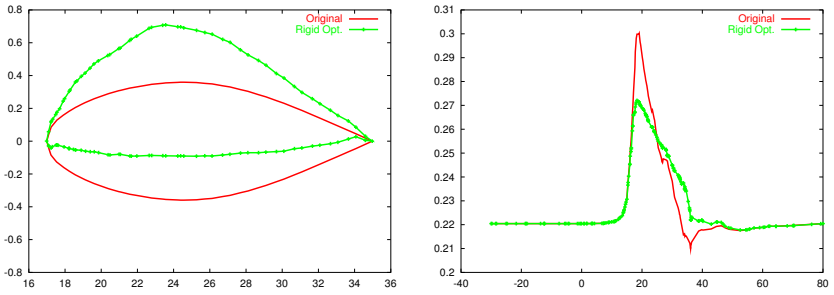

Figure 10: AGARD wing 445.6. Non-coupled optimization. Left, original and optimized (rigid) mid cross-sectional shapes or airfoils. Right, pressure below the original and the optimized rigid airfoils.

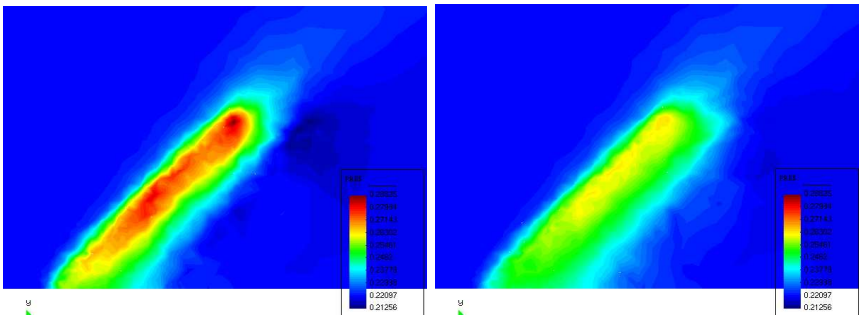

Figure 11: AGARD wing 445.6. Non-coupled optimization. Pressure distribution for a plane below the original and optimized (rigid) wings, left and right respectively.

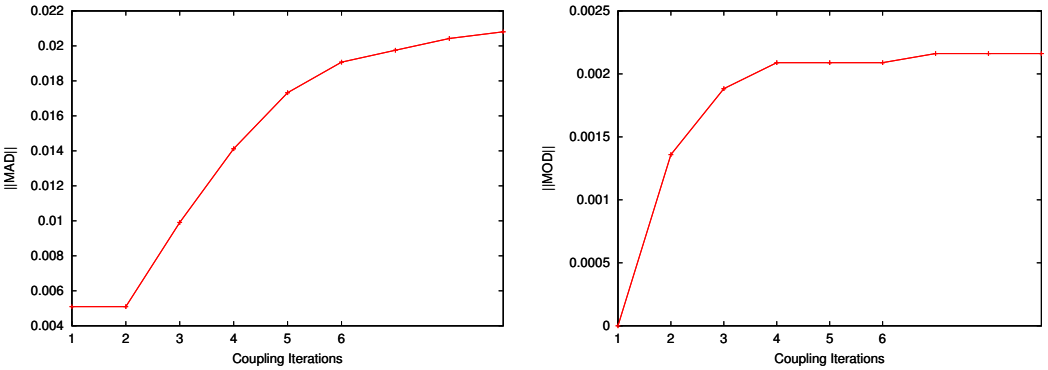

Figure 12: AGARD wing 445.6. Evolution of the mean aeroelastic displacements (||MAD||) and the mean optimization displacements (||MOD||) with the coupling iterations.

Fig. 12 shows the evolution of the mean aeroelastic displacement norm and the mean optimization displacement norm. As in the previous case, these norms are stabilized after some coupling iterations. The plots in Fig. 13 show the effects of the aeroelastic coupling in the optimization process. As for delta wing, the "target" lift is that of the original wing at initial incidence angle 3°. The curve labelled as "Coupling iteration 1" corresponds to the initial rigid wing optimization. After each of the 9 coupling iterations, the target is progressively reached. This is done by the combined effect of cambering and incidence angle variation. The final incidence angle is almost three

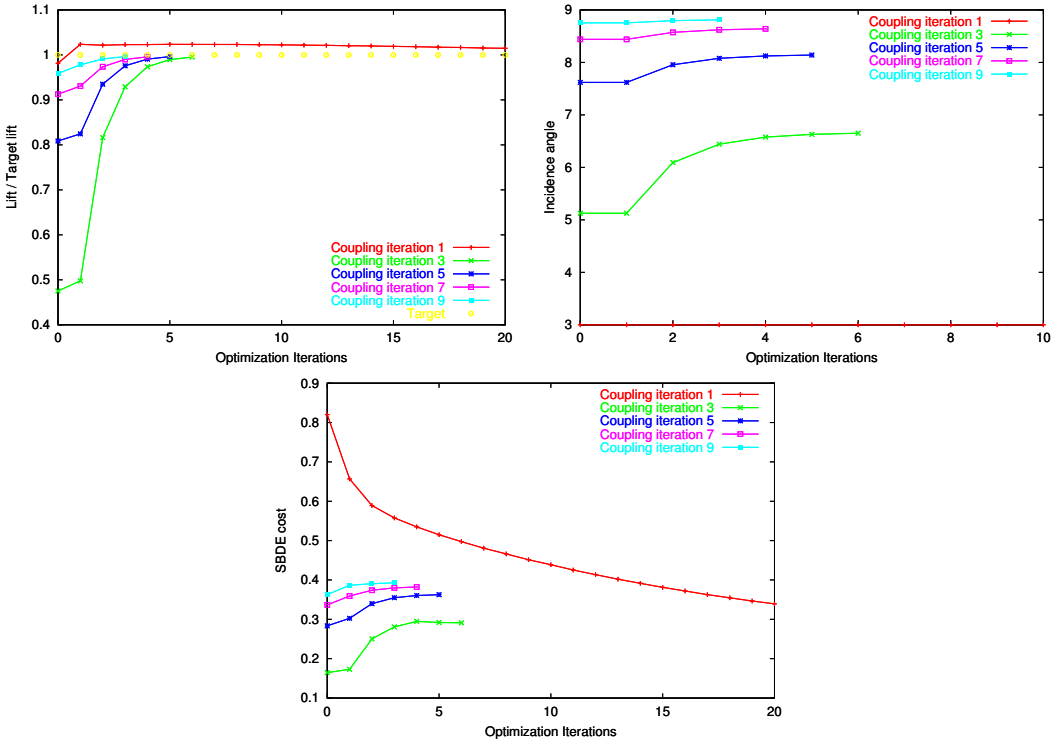

Figure 13: AGARD wing 445.6. Evolution of different parameters with the coupling iterations.

times as much as the initial one. This is the consequence of the large lost in lift due to the wing aeroelastic twist. The importance of this strong twist is obvious through the SBDE evolution (Fig. 13, bottom). Additionally to the lift loss, the aeroelastic twist produces a strong reduction in SBDE, independently of the deformation coming from the optimization method. Then, the algorithm tries to recover the lift while keeping the SBDE reduction. It is obvious that for this highly deformable wing, a much larger incidence angle is needed in order to recover the lift, which rises in turn the SBDE production. This results in a final SBDE that is very close to that of the rigid optimized wing, with a rather different at-rest geometry. In any case, the relative weights of these effects are controlled by the α's set. We have preferred to keep them equal to those of the delta wing for comparison purposes. The high flexibility of the wing at this supersonic regime is seen in Fig. 14.

6 Concluding remarks

In this paper, we have proposed a methodology for the shape optimization of flexible wings. This methodology is based on a two-step iterative procedure. At each coupling iteration an aeroelastic analysis is followed by an aerodynamic optimization. The second step takes the aeroelastic deformed shapes produced by the first step to compute the optimized shape. Both steps are connected through a controled deformation of the fluid volumic mesh in order to conform it to the optimized surface. The two-step iteration is repeated until the target is reached. The aeroelastic analysis is based on a classical loosely-coupled method which involves high fidelity aerodynamic and structural analysers. The shape optimizer is a "CAD-free" approach combined with a multi-level preconditioner which has good smoothing properties and transpiration conditions which characterize the shape optimization modifications.

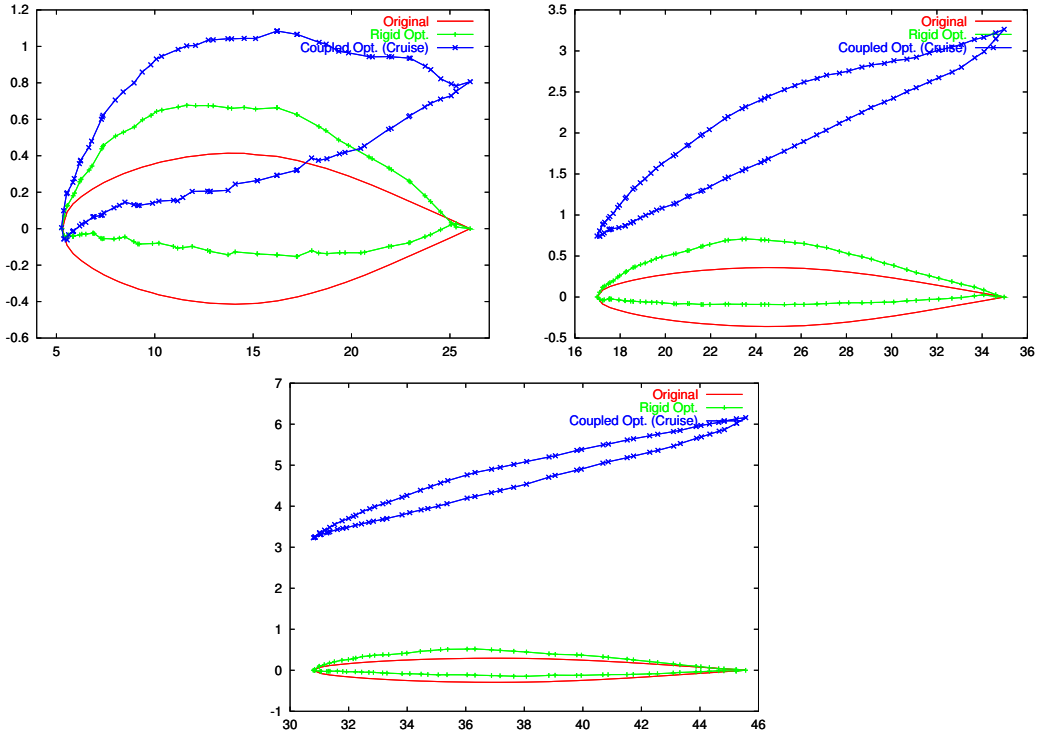

Figure 14: AGARD wing 445.6. Optimized wing. Clockwise: inboard, mid-wing and outboard cross-sectional cuts.

In contrast to a fully coupled optimization algorithm, the management of a three-field state system and thus a three-field adjoint one is avoided. On the aeroelastic side, no sensitivities are computed and a well-known fluid/structure interaction solver is virtually used as a black-box for performing the aeroelastic analysis. We have observed a convergent behavior of the scheme, which is reached after no more than 10 optimization/aeroelastic coupling iterations.

The proposed shape optimization methodology is applied to the reduction of the sonic boom production while preserving the aerodynamic performances of wings, taking into account the aeroelastic deformations suffered by wings in flight conditions. First a double-delta wing for a projected supersonic business jet is optimized in order to reduce its sonic boom downwards emission. The optimized shapes present very different transversal sections, according to their relative wing-span position. The influence of the aeroelastic deformations on the aerodynamic and sonic boom production optimization process is apparent. This fact can not be neglected, particularly when different flight regimes of a supersonic aircraft are considered. The aeroelastic effect is clearly seen when both rigid and coupled "at-rest" optimized shapes are compared. As a second application, the AGARD 445.6 is considered in order to demonstrate the robustness of the proposed optimization/aeroelastic coupling algorithm in the case of larger deformations. As for the delta wing, we also observe the aeroelastic effects on the coupled optimized shape.

The optimized shapes so-obtained are evaluated with the corresponding mesh deformation, which means that the transpiration approximation does not influence the evaluation of the flow and its performances, but only the identification of an optimum.

Since the shape at rest remains the central variable of the process, our algorithm extends to multi-point optimization, while traditional jig-shape methods do not apply well to that context.

We believe that the proposed methodology is also well-adapted to the cooperation between departmental tools in industrial context. Methods of this kind open the door to accurate multipoint shape optimization thanks to a complete, but not communication-intensive coupling, in a multidisciplinary cooperative optimization.

.

.

.

.

.

.

Acknowledgements

This work was partly supported by the Comite d'Orientation pour l'Avion Supersonique. Acces to parallel computing was provided by CINES.

References

[1] J.A. YOUNG, R.D. ANDERSON, and R.N. YURKOVICH. A description of the F/A-18E/F design and design process. *AIAA Paper 98-4701*, 1998.

[2] N. RADOVCICH and D.LAYTON. The F-22 structural/aeroelastic design process with mdo examples. Symposium on Multidisciplinary Analysis and Optimization. *AIAA White Paper*, 1998.

[3] P. BARTHOLOMEW. The role of mdo within aerospace design and progress towards an mdo capability. *AIAA Paper 98-4705*, 1998.

[4] J. SOBIESZCZANSKI-SOBIESKI and R.T. HAFTKA. Multidisciplinary aerospace design optimization: survey of recent developments. *Structural Optimization*, 14(1), 1997.

[5] AIAA Technical Committee for MDO. Current state of the art of multidisciplinary design optimization. AIAA White Paper, September 1991.

[6] R. SHUBIN. Application of Alternative Multidisciplinary Optimization Formulation to a Model Problem for Static Aeroelasticity. *Journal of Computational Physics*, 118:73–85, 1995.

[7] E. ARIAN. On the Coupling of Aerodynamic and Structural Design. *Journal of Computational Physics*, 135:83–96, 1997.

[8] A.C. TAYLOR, L.L. GREEN, P.A. NEWMAN, and M.M. PUTKO. Some advanced concepts in discrete aerodynamic sensitivity analysis. *AIAA Paper*, 2001-2529:1–10, 2001.

[9] J.C. NEWMAN, W.K. ANDERSON, and D.L. WHITFIELD. Multidisciplinary sensitivity derivatives using complex variables. Technical Report - CFD Laboratory - Mississippi State University MSSU-COE-ERC-98-08, July 1998.

[10] A.A. GIUNTA. Sensitivity analysis for coupled aero-structural systems. NASA Technical Report NASA/TM-1999-209367, August 1999.

[11] J. SOBIESZCZANSKI-SOBIESKI. Sensitivity of complex, internally coupled systems. *AIAA J.*, 28(1):153–160, 1990.

[12] K. MAUTE, M. NIKBAY, and C. FARHAT. Sensitivity analysis and design optimization of three-dimensional non-linear aeroelastic systems by the adjoint method. *Int. J. Numer. Meth. Engng.*, 56:911–933, 2003.

[13] J.J. ALONSO, J.R.R. MARTINS, J.J. REUTHER, R. HAIMES, and C.A. CRAWFORD. High-fidelity aero-structural design using a parametric CAD-based model. *AIAA Paper 03-3429*, 2003.

[14] J.R.R. MARTINS, J.J. ALONSO, and J.J. REUTHER. Aero-structural wing design optimization using high-fidelity sensitivity analysis. In Germany Cologne, editor, *In CEAS Conference on multi-disciplinary aircraft design optimization*, pages pages 211–226, 2001.

[15] N.M. ALEXANDROV and R.M. LEWIS. Dynamically reconfigurable approach to multidisciplinary problems. *AIAA Paper 03-3431*, 2003.

[16] H. HOENLINGER, J. KRAMMER, and M. STETTNER. MDO technology needs in aeroelastic structural design. *AIAA paper 98-4731*, 1998.

[17] J.T. ODEN, T. BELYTSCHKO, I. BABUSKA, and T.J.R. HUGHES. Research directions in computational mechanics. *Comp. Meth. Appl. Mech. Eng.*, 192:913–922, 2003.

[18] K. WILLCOX and S. WAKAYAMA. Simultaneous optimization of a multiple-aricraft family. *Journal of Aircraft*, 40(4):616–622, 2003.

[19] M. VAZQUEZ, B. KOOBUS, and A. DERVIEUX. Aerodynamical and sonic boom optimization of a supersonic aircraft. Technical Report RR-4520, INRIA, 2002. http://www-sop.inria.fr/rapports/sophia/RR-4520.html.

[20] M. VAZQUEZ, B. KOOBUS, and A. DERVIEUX. Multilevel optimization of a supersonic aircraft. *Finite Elements in Analysis and Design*, 2003.

[21] B. MOHAMMADI and O. PIRONNEAU. *Applied shape optimization for fluids*. Clarendon Press - Oxford, 2001.

[22] C. FARHAT, M. LESOINNE, and N. MAMAN. Mixed explicit/implicit time integration of coupled aeroelastic problems: three-field formulation, geometric conservation and distributed solution. *Int. J. Num. Meth. Fluids.*, 21:807–835, 1995.

[23] R. SEEBAS and B. ARGROW. Sonic boom minimization revisited. *AIAA Paper*, 98-2956:1–13, 1998.

[24] D.J. MAGLIERI and K.J. PLOTKIN. *Aeroacoustics of flight vehicles: theory and practice*. Acoustical Society of America, Publications, 1991.

[25] C. FARHAT. High performance simulation of coupled non-linear transient aeroelastic problems. AGARD Report R-807, October 1995. Special Course on Parallel Computing in CFD.

[26] C. FARHAT and M. LESOINNE. On the accuracy, stability and performance of the solution of three-dimensional non-linear transient aeroelastic problems by partitioned procedures. *AIAA paper 96-1388*, April 18-19, 1996.

[27] J. DONEA. An arbitrary lagrangian-eulerian finite element method for transient fluid-structure interactions. *Comput. Meths. Appl. Mech. Engrg.*, 33:689–723, 1982.

[28] C. FARHAT, C. DEGAND, B. KOOBUS, and M. LESOINNE. Torsional springs for two-dimensional dynamic unstructured fluid meshes. *Comput. Meths. Appl. Mech. Engrg.*, 163:231–245, 1998.

[29] A. DERVIEUX. *Steady Euler Simulations Using Unstructured Meshes*. Von Karman Institute Lecture Series, Von Karman Institute, 1985.

[30] J.A. SAMAREH. A survey of shape parametrization techniques. In USA Williamsburg, editor, *In CEAS International forum on Aeroelsaticity and Structural Dynamics*, pages pages 1–12, 1999.

[31] J. REUTHER and A. JAMESON. Aerodynamic Shape Optimization of Wing and Wing-Body Configurations Using Control Theory. AIAA Paper 95-0123, 1995. 33rd Aerospace Sciences Meeting and Exhibit.

[32] A. DERVIEUX, S. LANTERI, J.M. MALE, N. MARCO, N. ROSTAING-SCHMIDT, and B. STOUFFLET. New technologies for advanced three-dimensional optimum shape design in aeronautics. *Int. J. Num. Meth. Fluids.*, 30:179–191, 1999.

[33] F. COURTY, A.DERVIEUX, B. KOOBUS, and L. HASCOET. Reverse automatic differentiation for optimum design: from adjoint state assembly to gradient computation. Technical Report RR-4363, INRIA, 2002. http://www-sop.inria.fr/rapports/sophia/RR-4363.html.

[34] F. COURTY. *Optimisation Différentiable en Mécanique des Fluide Numérique*. PhD thesis, PhD thesis, Université d'Orsay, 2003.

[35] N. MARCO and A. DERVIEUX. Multilevel parametrization for aerodynamical optimization of 3D shapes. *Finite Elements in Analysis and Design*, 26:259–277, 1997.

[36] B. MOHAMMADI. Optimization of aerodynamic and acoustic performances of supersonic civil transports. In *Center for Turbulence Research. Proceedings of the Summer Program 2002*, 2002.

[37] J. D. ANDERSON. *Introduction to Flight*. Mc. Graw - Hill, 2000.

[38] C. HELD and A. DERVIEUX. One-shot airfoil optimisation without adjoint. *Computers and Fluids*, 31(8):1015–1049, 2002.

[39] E.C. YATES. AGARD standard aeroelastic configuration for dynamic response, candidate configuration i. - wing 445.6. *NASA TM-100492*, 1987.